aerospace

MDPI

Article

Combustion Visualization and Liquid Jet in Crossflow Analysis of H_2O_2/Kerosene Bipropellant Thruster

Suk Min Choi *,†, Sangwoo Jung, Vincent Mario Pierre Ugolini and Sejin Kwon

Department of Aerospace Engineering, Korea Advanced Institute of Science and Technology, 291, Daehak-ro, Yuseong-gu, Daejeon 34141, Republic of Korea; jsw747@kaist.ac.kr (S.J.); vincent.ugolini@kaist.ac.kr (V.M.P.U.); trumpet@kaist.ac.kr (S.K.)

* Correspondence: suk_min.choi@tu-dresden.de

† Current affiliation: Institute of Aerospace Engineering, Technische Universität Dresden, Marschnerstr. 32, 01307 Dresden, Germany.

Abstract: In the H_2O_2/Kerosene bipropellant thruster, a liquid fuel jet is transversely injected into a crossflow of hot oxygen and water vapor, catalytically decomposed from a liquid oxidizer. Due to the high temperature and oxygen-rich environment, kerosene is auto-ignited without the need for an additional ignition source. Hence, fuel trajectory and breakup processes play a significant role in determining the performance of the rocket engine. However, little effort has been made to analyze these characteristics during actual rocket engine operation, mainly due to its harsh operating conditions of high temperature and pressure. In this study, an optically accessible combustion chamber was prepared to visualize the trajectory and breakup processes of the liquid jet during rocket engine operation. Physical and chemical processes inside the chamber were recorded using a high-speed camera utilizing a shadowgraph technique along with chemiluminescence suppression. Hot-fire tests were performed using 90 wt.% hydrogen peroxide and Jet A-1 in various jet-to-crossflow momentum flux ratios. Test cases with water injection replacing fuel were conducted with varying momentum flux ratios to identify the effect of the combustion process on the liquid jet. The study revealed that the existing correlations for the liquid jet trajectory commonly used for designing the H_2O_2/Kerosene bipropellant thruster in the past induced significant errors and suggested that the radiation heat transfer from the combustion flame downstream could affect the breakup processes upstream. A new correlation was suggested that accurately predicts the liquid fuel jet trajectory of the H_2O_2/Kerosene bipropellant thruster.

Keywords: liquid jet in crossflow; hydrogen peroxide/kerosene bipropellant thruster; combustion visualization; parameter optimization

Academic Editor: Qingfei Fu

Received: 28 December 2024
Revised: 22 January 2025
Accepted: 29 January 2025
Published: 31 January 2025

Citation: Choi, S.M.; Jung, S.; Ugolini, V.M.P.; Kwon, S. Combustion Visualization and Liquid Jet in Crossflow Analysis of H_2O_2/Kerosene Bipropellant Thruster. *Aerospace* **2025**, *12*, 110. https://doi.org/10.3390/aerospace12020110

1. Introduction

Recent increases in space accessibility and advances in space mission complexity have led to the growing need for a storable, high-performance, in-orbit propulsion system. For such propulsion systems, hydrazine and its derivatives have been the most widely used propellants for their high performance and storability; however, they are highly toxic, carcinogenic, and flammable. Due to growing safety and health requirements and the resulting increase in development costs, numerous efforts have been made to replace these hazardous propellants with environmentally friendly, green propellants. Highly concentrated hydrogen peroxide is among the most promising candidates. Its low vapor pressure at room temperature leads to excellent stability and storability, making hydrogen

peroxide handling considerably easy. Unlike the commonly used storable propellants, hydrogen peroxide is a non-toxic, non-carcinogenic substance. Liquid hydrogen peroxide can be decomposed into gaseous products expressed as $H_2O_2(l) \rightarrow H_2O(g) + \frac{1}{2}O_2(g)$, an exothermic reaction with a heat of decomposition of 94.6 kJ $\cdot$ mol^{-1}.

To further enhance the capability of hydrogen peroxide, several studies have been performed in recent years worldwide on utilizing a liquid hydrocarbon (HC) as a fuel for bipropellant propulsion systems. The University of Purdue developed an H_2O_2/Kerosene staged-bipropellant rocket engine and performed studies on combustion chamber sizing and hypergolicity tests [1,2]. The Korea Advanced Institute of Science and Technology developed a similar bipropellant engine and conducted research related to fuel injection and oxidizer film cooling technologies [3–5]. The Warsaw Institute of Aviation has developed and demonstrated a hydrogen peroxide bipropellant propulsion system using various types of fuel, including kerosene, TMPDA, and ethanol and established multidisciplinary optimized design procedures [6–9]. The University of Padova [10] investigated the combustion chamber cooling mechanism using double co-spinning counter-flowing vortex flow. H_2O_2/HC bipropellant propulsion systems exhibit an excellent volumetric specific impulse comparable to the high-performance yet toxic hydrazine bipropellants, making them suitable for in-orbit propulsion systems. The adiabatic decomposition temperature of the gaseous product of the highly concentrated hydrogen peroxide is higher than the auto-ignition temperature of major HC fuels. This feature simplifies the H_2O_2/HC bipropellant propulsion system by eliminating the need for a separate ignition system.

Figure 1 illustrates the operational concept of the H_2O_2/HC bipropellant thruster. Liquid hydrogen peroxide is first injected into the catalyst reactor, where it is catalytically decomposed into the gaseous products of hot oxygen gas and water vapor. The liquid fuel is then injected into the product gas and undergoes breakup processes of atomization, vaporization, and mixing. As the mixture gas is well above the auto-ignition temperature, the combustion process occurs spontaneously. The combustion product gas travels through the nozzle and creates thrust.

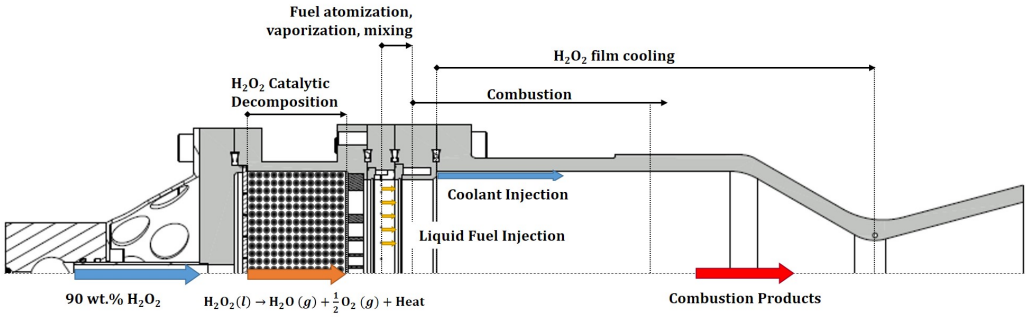

Figure 1. Operation concept of H_2O_2/HC bipropellant thruster.

For the injection of liquid fuel, transverse injection is known to promote stable and efficient combustion, thus being the most widely selected approach in the design of H_2O_2/HC bipropellant thrusters. This injection approach is utilized to enhance system performance when there is a low jet-to-crossflow momentum flux ratio present. The optimal oxidizer-to-fuel (OF) ratio, which involves H_2O_2 and kerosene—a widely used hydrocarbon fuel—typically ranges from 7 to 7.5, contingent upon the oxidizer's concentration. Consequently, this propellant pairing is well suited for adopting the transverse injection technique. As shown in Figure 2, a liquid jet introduced into the gaseous crossflow experiences aerodynamic forces that intensify the surface instabilities of the liquid column, thus dismantling it into ligaments and further into droplets.

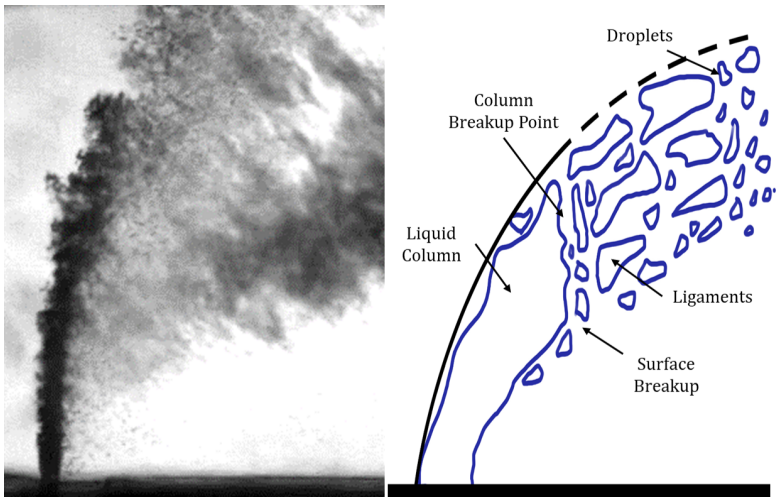

Figure 2. High-speed image (**left**) and schematic diagram (**right**) of liquid jet in crossflow.

Previous research has shown that the liquid jet in crossflow (LJICF) phenomenon is crucial to the performance of the H_2O_2/HC bipropellant propulsion system. Sisco et al. [2] analyzed the characteristics of auto-ignition in relation to jet trajectory and predicted that excessive penetration of the fuel jet could heighten the risk of auto-ignition failure. Heo et al. [4] examined how jet penetration impacts combustion efficiency and proposed that a penetration depth between 44% and 72.4% of the chamber radius is most suitable for fuel injector design. For these studies, empirical correlations were used by researchers to estimate the jet trajectory as suggested by Wu et al. [1,2,4,11,12]. Wu developed his correlation for the trajectory of a jet by introducing different liquids into a subsonic gas at standard temperature and pressure (STP). The locations of the liquid column, from the point of injection to where it fractures, are aligned with the general form of the jet trajectory equation, which is predominantly influenced by the momentum flux ratio between the jet and the crossflow (q), as illustrated in Equation (1). Similarly, Cieliski et al. performed cold flow experiments to observe the LJICF phenomenon to devise the design configuration for a throttleable liquid propulsion demonstrator[7].

$$\begin{gathered} z/d_j = 1.37q^{0.5}(x/d_j)^{0.5} \\ (q: 3.4-185, \quad We_g: 57-1180, \quad x/d_j: 0-12) \end{gathered} \tag{1}$$

The conditions within the combustion chamber are characterized by elevated temperature and pressure (HTHP), along with an intense combustion process. This results in significant differences in the properties of both liquids and gases, causing notable distortions in the estimation of jet trajectory and penetration depth based on prior studies. A limited number of investigations have been conducted to develop correlations for jet trajectories under HTHP conditions [13–15]. Eslamian et al. investigated the atomization and trajectories of a water jet introduced into a subsonic crossflow of air with pressures reaching 5 bar and temperatures of 573 K, with a focus on the influence of the spray plume's shape and area [16]. Amighi et al. carried out similar research by injecting different types of liquids into a subsonic air crossflow under conditions up to 300 °C and 5.2 bar, and they suggested using the Ohnesorge number in the correlation of jet trajectories [17]. Nonetheless, these studies were performed at pressures and temperatures peaking at 20 bar and 650 K, without including the combustion process, which are substantially lower than the actual conditions in a rocket engine combustion chamber.

In this study, the LJICF phenomenon was observed within the combustion chamber of an H_2O_2/kerosene bipropellant thruster during hot-fire testing. A combustion chamber equipped with a film cooling optical window was employed for chemiluminescence-

suppressed shadowgraph imaging to visualize the liquid column and its breakup process. Test campaigns varying the jet-to-crossflow momentum flux ratios were conducted by adjusting the oxidizer tank pressure, thereby modifying the crossflow gas mass flow rate. Two distinct liquids (water and kerosene) were injected using a transverse fuel injector to determine the effects of combustion and subsequent flame radiation on the LJICF trajectory. The images collected from the hot-fire tests were analyzed to evaluate empirical correlations proposed in previous studies. Furthermore, a new correlation was developed based on the experimental data, tailored for application under HTHP conditions with an associated combustion process.

2. Experimental Setup

2.1. 100 N H_2O_2/Kerosene Bipropellant Thruster

A bipropellant thruster, capable of producing 100 N of thrust at sea level, was engineered utilizing 90 wt.% hydrogen peroxide as the oxidizer and Jet A-1 as the fuel. The hydrogen peroxide's quality utilized in hot-fire testing met the specifications of MIL-PRF-16005F [18]. The design parameters and anticipated performance metrics were derived using the NASA Chemical Equilibrium and Applications (CEA) code [19]. Table 1 displays the design parameters of the H_2O_2/Kerosene bipropellant thruster, while Figure 3 illustrates the designed thruster along with its operational schematics.

Table 1. Design parameters of 100 N H_2O_2/Kerosene bipropellant thruster.

Parameter	Value
Oxidizer	90 wt.% H_2O_2
Fuel	Jet A-1
Oxidizer mass flow rate	28.0 g/s
Fuel mass flow rate	4.0 g/s
OF ratio	7.0
Chamber pressure	20 bar
Maximum chamber temperature	2730 K
Maximum crossflow temperature	1032 K
Test section dimensions	20 mm × 20 mm
Test section length	95 mm
Fuel injector orifice diameter	0.564 mm
Length-to-diameter ratio of fuel injector	8.0

As illustrated in Figures 3 and 4, a singular circular orifice fuel injector with an orifice diameter of 0.564 mm was positioned downstream from the catalytic reactor. The design did not incorporate a rearward-facing step for flame holding to eliminate any potential impact of flow recirculation on the LJICF phenomenon. On each side of the combustion chamber, two optical windows, each 15 mm thick and crafted from NC-200 quartz, were installed and sealed using Klinger gaskets and Viton o-rings. The flexibility of these sealing components mitigated structural vibrations on the windows, thereby reducing the risk of cracks. Between the catalytic reactor and the combustion chamber, a connector was installed with a 1 mm thick slot on both sides for film cooling N_2 gas injection.

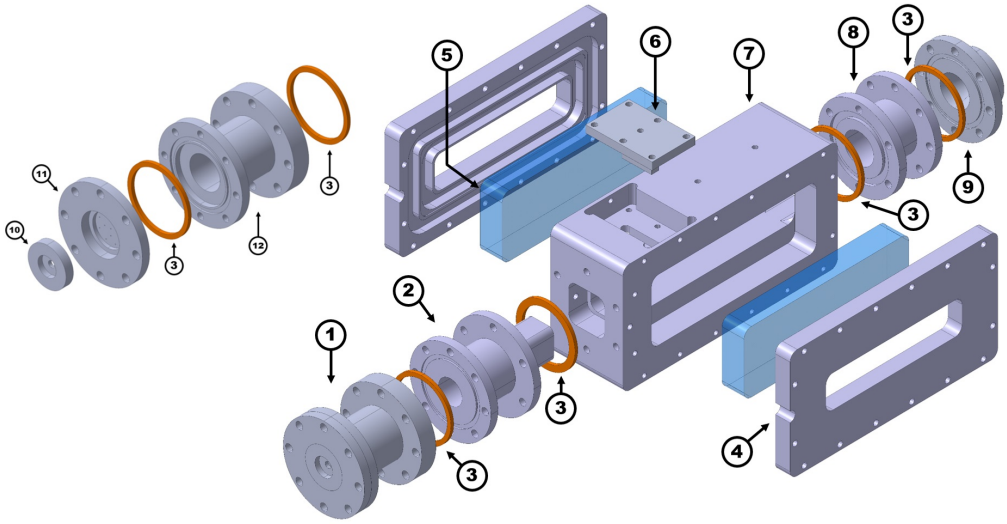

Figure 3. Parts breakdown of the H_2O_2/Kerosene bipropellant thruster (1: catalyst reactor; 2: connector; 3: copper gasket; 4: exterior flange; 5: quartz window; 6: fuel injector; 7: combustion chamber; 8: connector; 9: nozzle; 10: pipe connector; 11: injector flange; 12: catalyst bed).

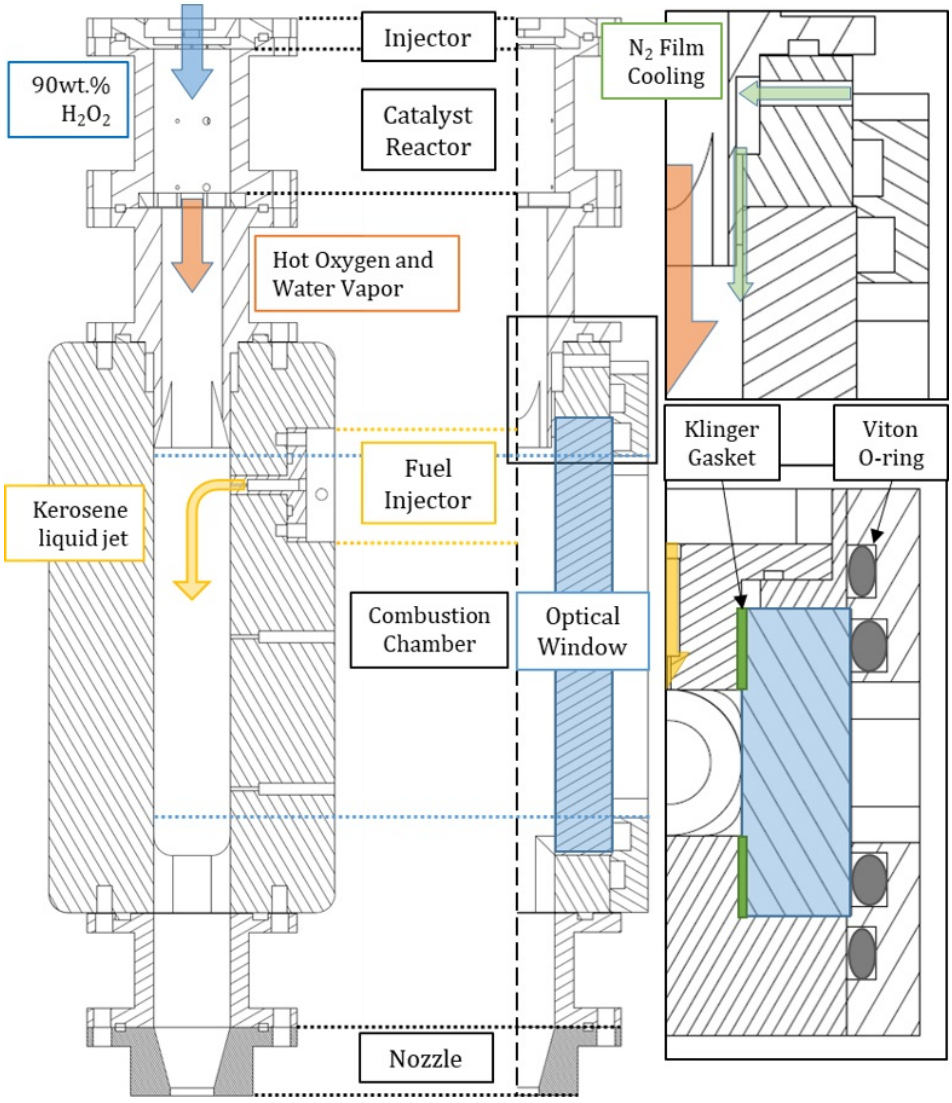

Figure 4. H_2O_2/Kerosene bipropellant thruster design schematics.

The NC-200 quartz material is capable of withstanding compression pressures up to 1.1 GPa and temperatures as high as 1600 K. Nevertheless, combustion temperatures can rise to 2700 K, surpassing the material's limits. To mitigate thermal shock cracks, N_2 gas film cooling was applied to the interior surface of the windows. This gas cooling method also helped reduce soot build-up from incomplete combustion. As shown in Figure 5, CFD analysis using ANSYS Fluent® Release 16.1 simulated the worst-case scenario of crossflow with combustion gas temperatures. The analysis verified that the N_2 gas effectively reduced the optical window's temperature to below 1000 K, which is safely within its operational range. Importantly, the study confirmed that the film cooling gas addition does not alter the mole fraction in areas where primary breakup and combustion take place, thus indicating minimal disruption from the N_2 gas film cooling.

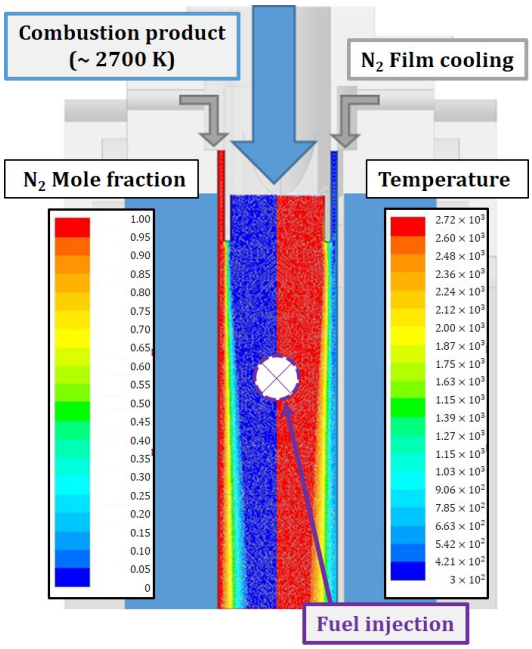

Figure 5. CFD analysis using ANSYS Fluent® to calculate mass fraction of N_2 species (**left**) and temperature (**right**).

Lastly, the $MnO_2/PbO/Al_2O_3$ catalyst was selected for the decomposition of the liquid oxidizer. Commercially available γ-alumina pellets were crushed, polished, and screened with a sieve with a mesh size in the range 10–16 (1.19–2.20 mm) to be used as the catalyst support. The active agents of the catalyst were manganese oxide and lead(II) oxide, which were attached to the surface of the catalyst support using the wet impregnation method. The particles were immersed in a precursor, sodium permanganate solution ($NaMnO_4$), and lead(II) oxide solution, then dried and calcinated. Impurities, such as sodium ions, were washed out with distilled water, followed by a final calcination process. The size of the catalyst bed was determined following the design optimization criteria suggested by Jung et al. [20]. The images of the fabricated and integrated combustion chamber of the H_2O_2/Kerosene bipropellant thruster are shown in Figure 6.

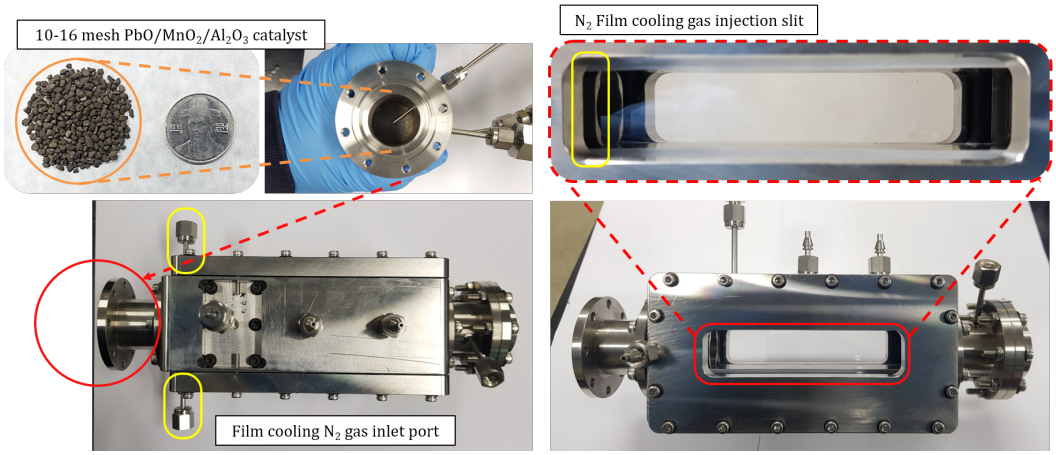

Figure 6. Images of H_2O_2/Kerosene bipropellant thruster and its components.

A schematic diagram of the propellant feeding system and an actual image of the experimental setup are shown in Figure 7 and Figure 8, respectively. The tanks of each propellant are pressurized by a high-pressure N_2 gas. The flow of the propellants was controlled using pneumatic and solenoid valves. The temperature and pressure data were acquired at a rate of 40,000 samples and 80 samples per second, respectively, using a data acquisition system (Chassis: SCXI-1000; Voltage module: SCXI-1120 with SCXI-1320 terminal; Thermocouple module: SCXI-1112, National Instruments Corporation, Austin ,TX, USA) equipped with the LabVIEW program. K-type thermocouples (Omega Engineering Inc., Norwalk, CT, USA) and pressure transducers (Sensys Inc., Ansan, Republic of Korea, and Kulite Inc., Leonia, NJ, USA) were used to measure temperature and pressure. The mass flow rate of the propellants was obtained utilizing the orifice plate differential pressure mass flow meter.

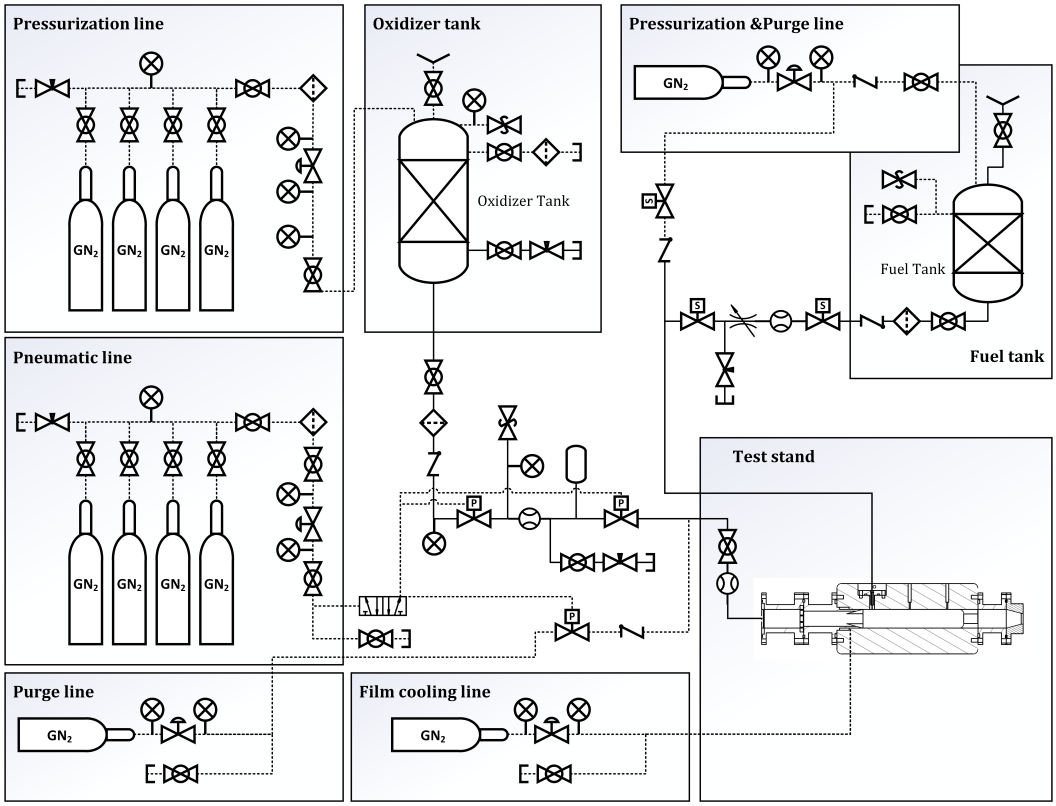

Figure 7. Schematic diagram of propellant feeding system at KAIST [21].

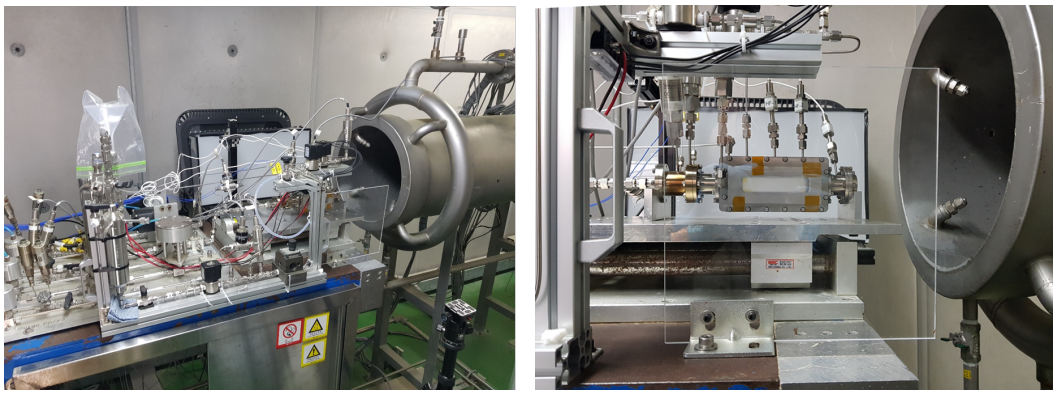

Figure 8. Propellant feeding system and thruster experimental setup (**left**) and combustion chamber visualization setup (**right**).

2.2. Combustion Visualization Setup

In this study, the backlit shadowgraph technique with chemiluminescence suppression was used to visualize the LJICF phenomenon. Shadowgraph is an optical method that reveals the nonuniformities of media. As the liquid mostly blocks the transmission of light, it is possible to effectively distinguish and detect the liquid jet from gaseous crossflow. Additionally, to acquire a clear image, it is necessary to suppress the chemiluminescence generated by the combustion flame. The flame radiation spectrum for the oxygen–kerosene combustion process illustrated by Harrje et al. [22] reveals that the peak intensity of radiation occurs at wavelengths of approximately 300, 420, and 500 nm caused by OH, CH, and C_2 radicals, respectively. It is impossible to block all flame radiation within the visible light spectrum due to the carbon continuum; however, it is possible to minimize the effect by filtering all but a narrow wavelength bandwidth of 450–500 nm . In this study, a high-power blue LED of 400–500 nm wavelength was used as a backlit illumination device. The light diffuser panel was mounted in front of the blue LED arrays to evenly distribute the intensity of the floodlight. A BP470 blue bandpass filter (Midwest Optical Systems Inc., Palatine, IL, USA) with a bandpass spectrum of 425–495 nm was used to filter combustion-induced chemiluminescence. As a result, the bandpass spectrum of 425–495 nm can be observed through the visualization setup. To obtain visual data, FASTCAM UX-100 (Photron Inc., Tyokyo, Japan) was used at 4000 frames per second, 1280 × 1024 resolution, and 1/200,000 shutter speed. The conceptual schematics of the shadowgraph visualization setup and the images from the test stand are shown in Figures 9 and 10. A scale bar was inserted in the combustion chamber before the experiment to derive the actual spatial position of the liquid jet from the recorded images.

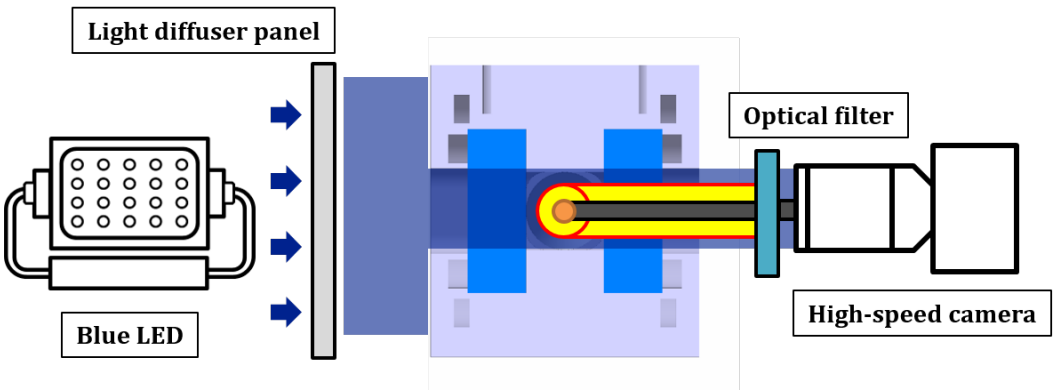

Figure 9. Conceptual schematics of shadowgraph visualization of combustion chamber with chemiluminescence suppression.

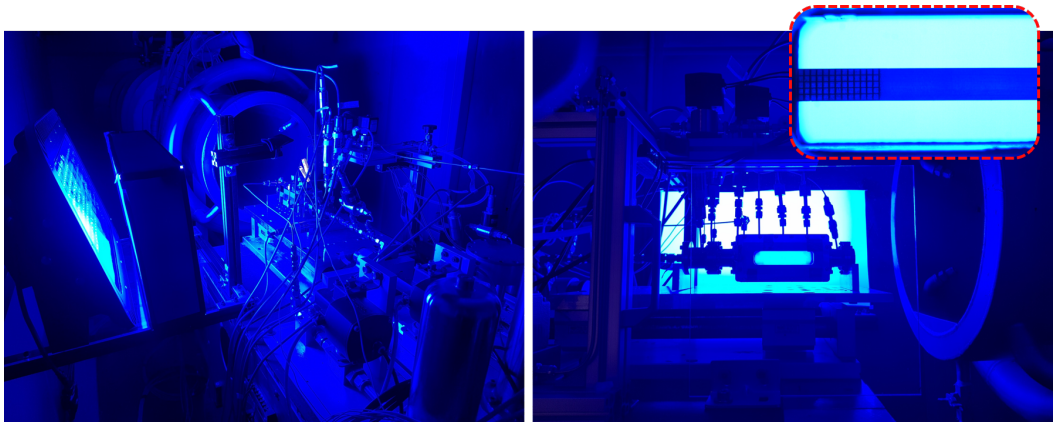

Figure 10. Propellant feeding system and thruster experimental setup (**left**) and combustion chamber visualization setup (**right**) with chemiluminescence suppression.

3. Hot-Fire Tests

3.1. Mono-Mode Operation

The validation of the H_2O_2/Kerosene bipropellant thruster, propellant feeding system, and visualization setup was initially carried out in mono-mode operation. During mono-mode, fuel was not introduced via the injector; solely liquid hydrogen peroxide was supplied to the catalyst reactor. The data presented in Figure 11 confirmed the success of the mono-mode test. In Figure 11a, pressure data were collected from 13 locations within the propulsion system, encompassing the tank pressures, feed lines, both mass flow meter (MFM) ports, the catalytic reactor, the combustion chamber, and the coolant injection port. To account for possible malfunctions of pressure transducers under extreme conditions, redundant observations were made for the combustion chamber pressure, as can be seen from the data of the p_3^{cc}. It was noted that a stable pressure in the combustion chamber was maintained at about 13 bar. Figure 11b indicates that the temperature downstream of the catalytic reactor (T_{CatBed_1}) reached a near-perfect adiabatic decomposition temperature of 1050 K, with no leakage detected at the optical window. Due to the incomplete decomposition at the upstream of the reactor, (T_{CatBed_2}) was observed to be lower than the adiabatic decomposition temperature. The window exhibited durability under mono-mode conditions even without the application of N_2 gas film cooling, suggesting that thermal shock cracking can be prevented by keeping the internal surface temperature of the optical window below 1050 K. When N_2 gas was introduced, water vapor from decomposition products condensed, reducing the visibility of the window, as depicted in Figure 12. However, this reduction in visibility was minimized during bi-mode operation with fuel injection, as the heat produced by the combustion flame effectively mitigated the condensation.

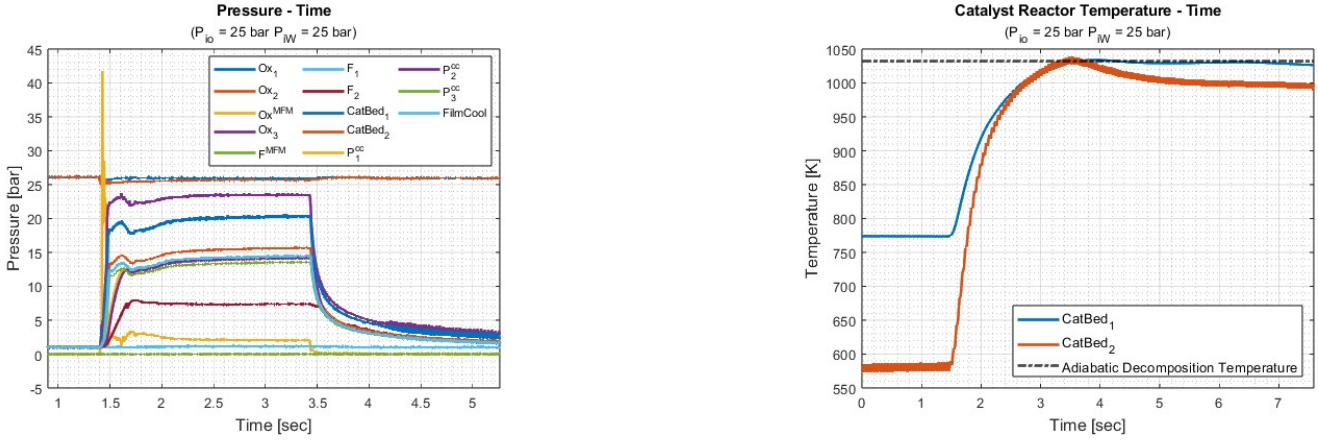

(**a**) (**b**)

Figure 11. Pressure measurement data (**a**) and temperature measurement data (**b**) from the mono-mode operation for experimental setup validation.

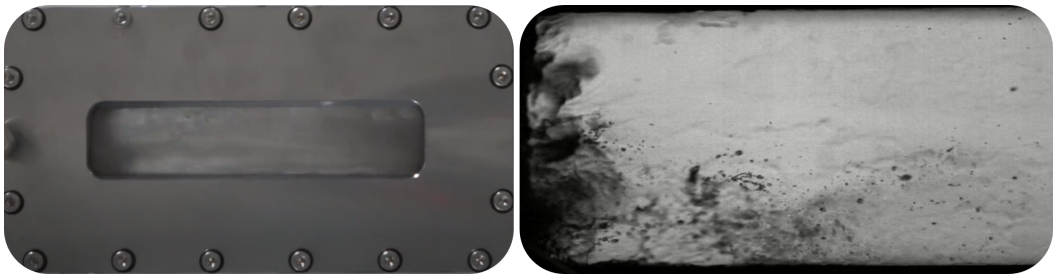

Figure 12. Recorded images of mono-mode operation using visualization chamber.

3.2. Bi-Mode Operations

Before the bi-mode hot fire tests commenced, a preliminary test campaign was executed using a series of dummy windows to define the operating conditions of the N_2 gas film cooling system. Two dummy walls, each 15 mm thick and made of stainless steel, were equipped with thermocouples extending to the interior surface of the combustion chamber, as illustrated in Figure 13. Subsequently, the N_2 injection pressure required to establish a gas mass flow rate adequate to prevent window overheating was iteratively examined.

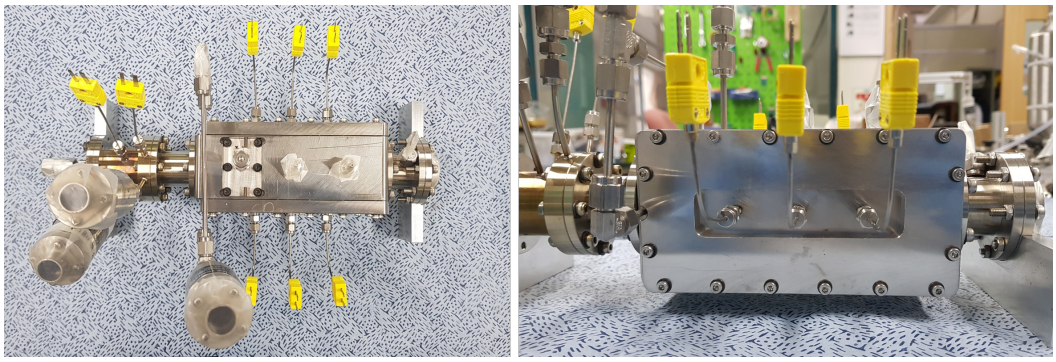

Figure 13. H_2O_2/Kerosene bipropellant thruster integrated with dummy windows.

Bi-mode operations were performed in two test campaigns utilizing different liquids injected via the fuel injector: kerosene and water. Initially, the bi-mode test campaign for fuel injection was executed under various jet-to-crossflow momentum flux ratios as presented in Table 2. Variations in the jet-to-crossflow momentum flux ratio (q) were accomplished by modifying the pressure in the oxidizer tank, thereby adjusting the mass

flow rate of the decomposition product gas passing through the combustion chamber. It was determined that pressures of 28 bar and 25 bar must be applied to the oxidizer and fuel tanks, respectively, to achieve the intended chamber pressure of 20 bar. The disparity observed between the predicted operating conditions, as presented in Table 1, is likely due to the reduced chamber temperature combined with the low-temperature N_2 coolant gas. Additional test cases depicted in the table were selected to have data points deviating slightly from the standard operating conditions to examine the LJICF trajectory and evaluate the current correlations.

Table 2. Hot-fire test conditions for fuel injection bi-mode operation.

P_{io} [bar] **P_{iF} [bar]**	**25** **25**	**28** **25**	**32** **25**	**36** **25**
Test label	25(HP)25(F)	28(HP)25(F)	32(HP)25(F)	36(HP)25(F)
P_{ch} [bar]	18.0	20.0	22.4	24.5
ROF	7.06	9.23	10.21	10.63
$\dot{m}_{Ox}$ [g/s]	32	35	40	44.4
$\dot{m}_F$ [g/s]	4.54	3.79	3.90	4.18
q	300.5	194.6	177.3	179.7

Subsequently, the bi-mode water injection test campaign was executed according to the test conditions outlined in Table 3. This bi-mode water injection operation allows for the preservation of crossflow characteristics while examining the impact of combustion and resultant radiative heat transfer on the LJICF phenomenon. Each test case is labeled using the format P_{io}(HP)P_{iL}(L), where P_{iX} denotes the tank pressure of the X propellant in bar, and L indicates the type of liquid introduced via the fuel injector, where F stands for fuel and W for water. Both fuel and water injection test campaigns were conducted for a separate day, employing the same catalyst throughout each test campaign, and were performed in order of increasing oxidizer tank pressure test cases.

Table 3. Hot-fire test conditions for water injection bi-mode operation.

P_{io} [bar] **P_{iW} [bar]**	**20** **25**	**25** **25**	**30** **25**
Test label	20(HP)25(W)	25(HP)25(W)	30(HP)25(W)
P_{ch} [bar]	8.7	12.6	16.5
ROF	-	-	-
$\dot{m}_{Ox}$ [g/s]	22.8	34.1	45.4
$\dot{m}_W$ [g/s]	10.3	5.1	5.8
q	1170.4	187.8	178.1

The bi-mode operation was conducted sequentially as depicted in Figure 14. As can be seen in the operation sequence, the bi-mode operation was gradually transitioned from and to the mono-mode to prevent sudden temperature changes, thus minimizing the risk of thermal shock cracking of the optical window. N_2 gas film cooling was activated throughout the 10 s of oxidizer duration. The high-speed camera recorded the images for nearly 1 s (approximately 4000 images) during the 3-second bi-mode operation.

As a result of the bi-mode test campaign, all test cases succeeded in auto-ignition as shown in Figure 15. As illustrated in Figure 16, the LJICF phenomenon is only observable with the proper chemiluminescence suppression due to the high-intensity flame radiation. Additionally, in the gray-scale image, a dark region could be seen downstream of the liquid jet, where soot produced from the locally low OF ratio condition obscured the backlit

illumination. In the raw image, the corresponding site appears as a bright light, consistent with the soot in the flame emitting light in the range from 700 nm to the mid-infrared spectrum. On the other hand, the bright zone located in the upper and lower parts of the main soot generation was likely to be caused by either CH or C_2 radicals caused by the locally high OF ratio condition.

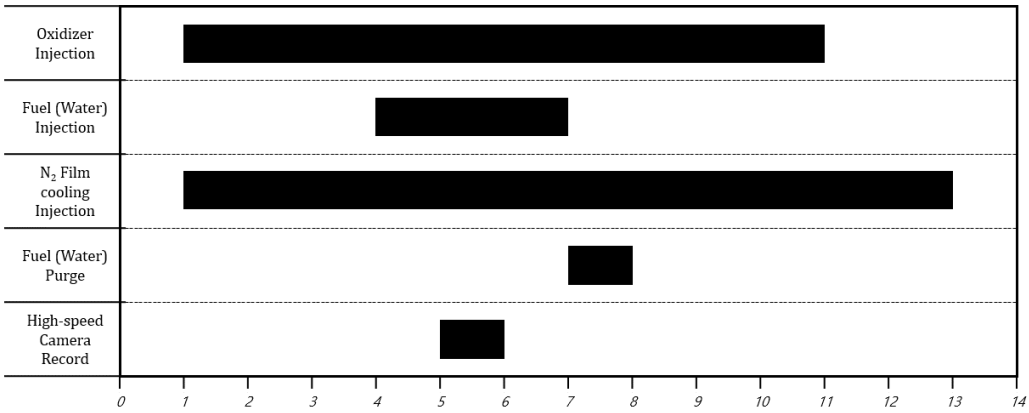

Figure 14. Bi-mode operation sequence.

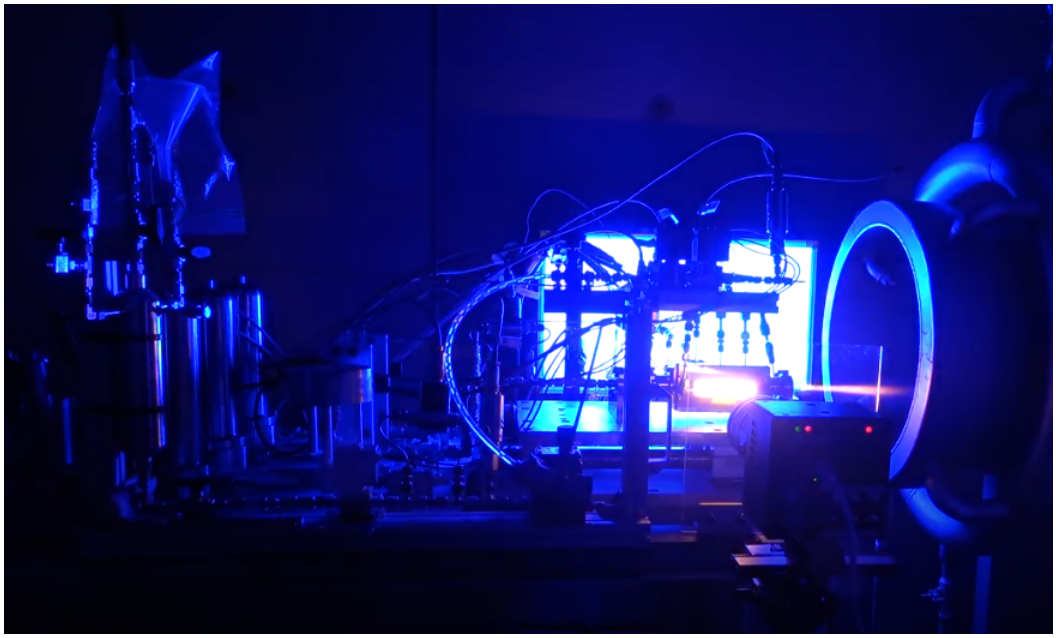

Figure 15. Hot-fire test of H_2O_2/Kerosene bipropellant thruster.

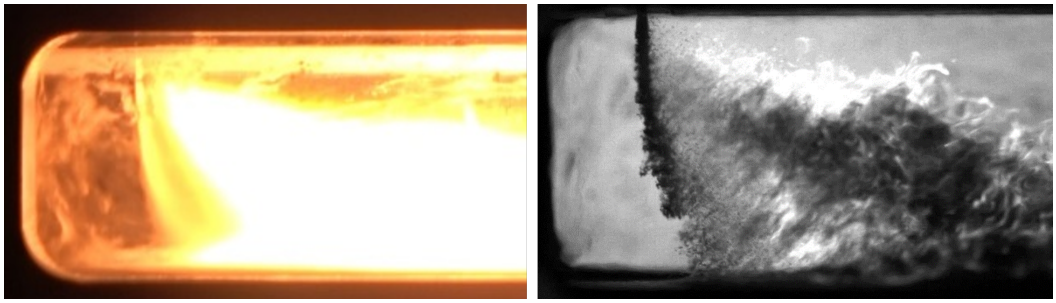

Figure 16. Effect of chemiluminescence imaging in shadowgraph images for observing the combustion process.

Figure 17 shows the pressure and temperature measurement data obtained from the fuel injection bi-mode operation with the oxidizer tank pressure of 25 bar (Figure 17a,b) and 32 bar (Figure 17c,d). Pressure at the combustion chamber changed following the operation sequence explained in Figure 14 and achieved a nominal value of 19–23 bar as designed without significant combustion instability. The temperature downstream of the catalytic reactor reached the adiabatic decomposition temperature of 90 wt.% hydrogen peroxide, indicating the complete decomposition of the injected liquid oxidizer.

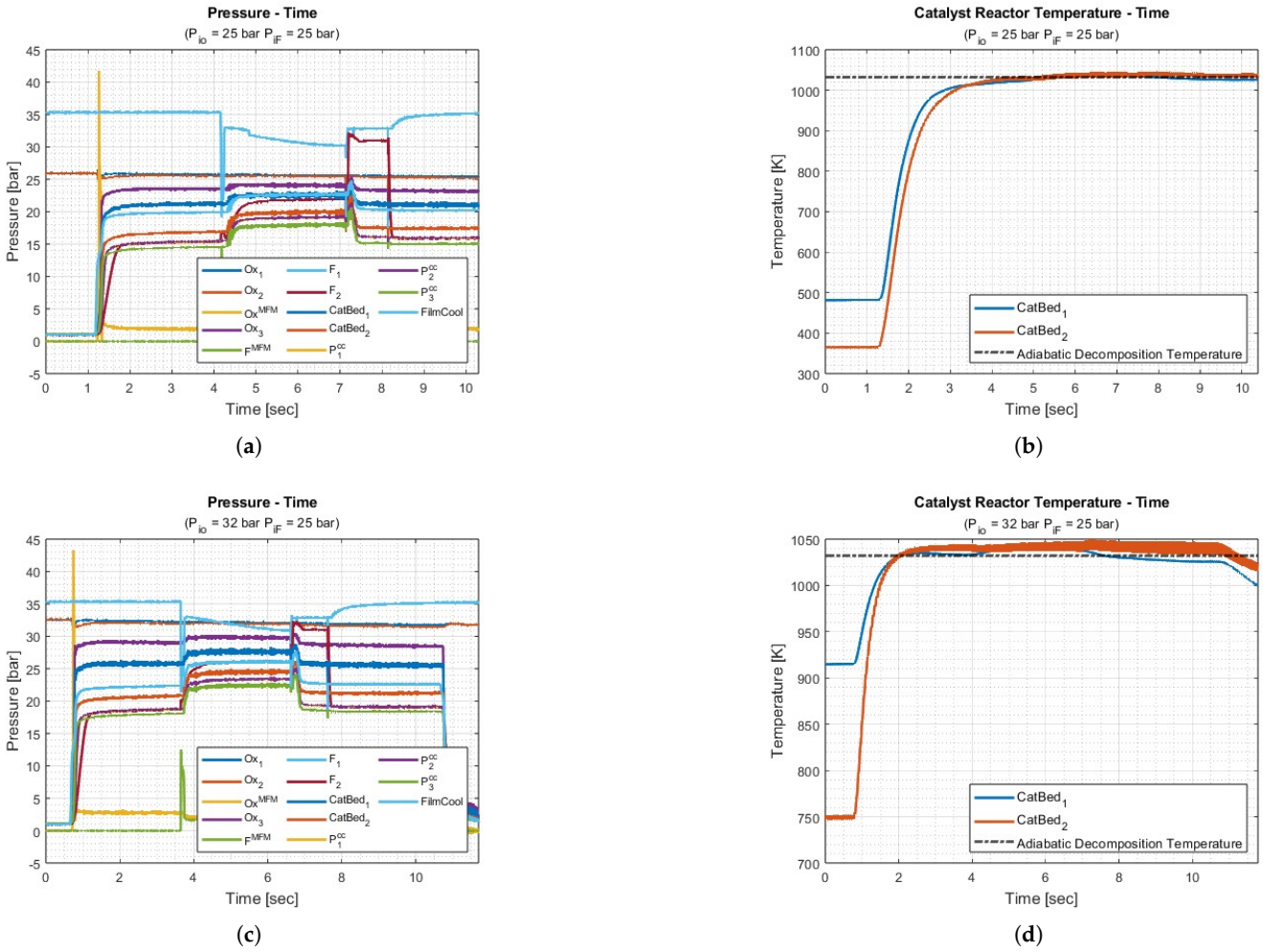

Figure 17. Pressure measurement data (**a**) and temperature measurement data (**b**) for fuel injection bi−mode operation at $P_{io} = 25$ bar, pressure measurement data (**c**) and temperature measurement data (**d**) for fuel injection bi−mode operation at $P_{io} = 32$ bar condition

Figure 18 illustrates the pressure and temperature measurement data obtained from the water injection bi-mode operation with an oxidizer tank pressure of 30 bar. The chamber pressure did not experience any notable pressure disturbance or increase in pressure during water injection and achieved a nominal pressure of 16–17 bar. The temperature downstream of the catalytic reactor reached the adiabatic decomposition temperature of 90 wt.% hydrogen peroxide, indicating the complete decomposition of the injected liquid oxidizer.

Figure 19 illustrates the intensity of the pressure perturbation at the catalyst bed downstream and the chamber for both hot-fire test campaigns. Here, P_{cc} and P_{cb} represent the pressure measurement taken at the combustion chamber and the catalytic reactor. Each test campaign, fuel and water injection, consists of four and three consecutive hot-fire tests using identical catalyst loaded into the reactor. Table 4 reveals a slight rise in

pressure perturbation progressively throughout the test campaigns. This is probably due to the slow deterioration of the catalyst, yet the reactor successfully decomposed the injected liquid oxidizer, keeping perturbations minimal. However, the heightened pressure perturbation could potentially destabilize the breakup processes of the liquid jet. This issue was mitigated by employing the time-averaged value of the optical measurement data, which will be further elaborated on in Section 4.1.

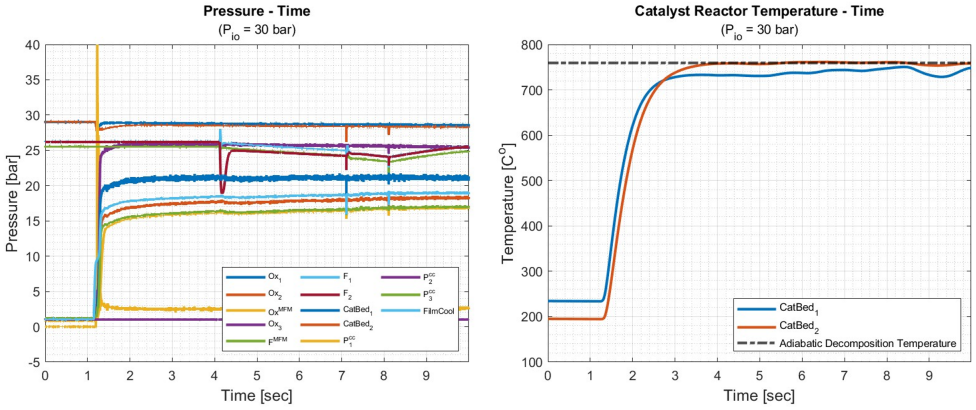

Figure 18. Pressure and temperature measurement for water injection bi−mode operation for $P_{io} = 30$ bar condition.

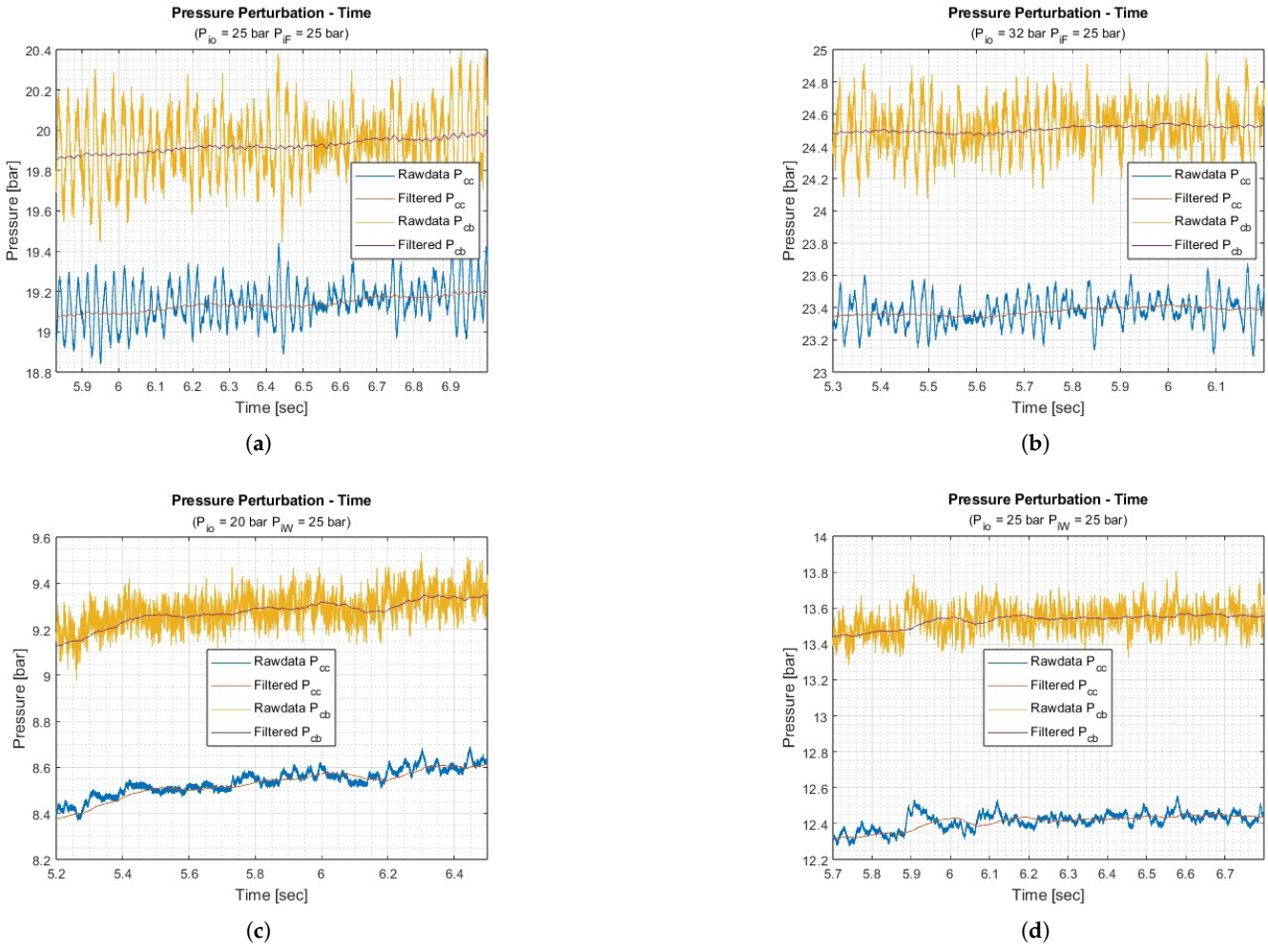

Figure 19. Pressure perturbation changes according to the consecutive operation for test cases (**a**) 25(HP)25(F), (**b**) 32(HP)25(F), (**c**) 20(HP)25(W), and (**d**) 25(HP)25(W).

Table 4. Intensity of the pressure perturbation at the catalyst bed downstream and chamber in each test case.

Case	MinMax (P'_{CB})	MinMax (P'_{CC})
25(HP)25(F)	0.9383 bar	0.5641 bar
28(HP)25(F)	0.9393 bar	0.5824 bar
32(HP)25(F)	1.0009 bar	0.5809 bar
36(HP)25(F)	1.2122 bar	0.7238 bar
20(HP)25(W)	0.3936 bar	0.1432 bar
25(HP)25(W)	0.5964 bar	0.3739 bar
30(HP)25(W)	0.6755 bar	0.3136 bar

4. Combustion Visualization

4.1. Image Processing

The raw images obtained from the combustion chamber were examined to observe the LJICF phenomenon. As shown in the left image of Figure 20, the flawless visualization image contains several features to be recognized. The liquid column can be distinguished as a dark vertical line starting from the fuel injection orifice. The primary breakup point can be specified as the other end of this column. Since the forced convection by the crossflow is the unsteady process and induces perturbation of the primary breakup point, an average value was taken over the time span of optical measurement to designate the breakup point corresponding to each test case. The small particles next to the column represent the droplet generation as a result of the surface breakup process. The dark zone on the right side is suspected to be created by the soot particles from the incomplete combustion process. On the contrary, the bright zone on top and bottom of the soot-induced dark zone most likely coincides with the stoichiometric reaction zone and is caused by the radiation of CH radicals. In some test cases, the visualization images might be poor in quality as shown in the images in the middle and on the right of Figure 20. Images obtained from the later part of the test campaign are often disrupted by continuous deposition of soot on the interior surface of the optical window, even with the N_2 film cooling. In addition, slight dislocation of the high-speed camera can lead to capturing out-of-focus images.

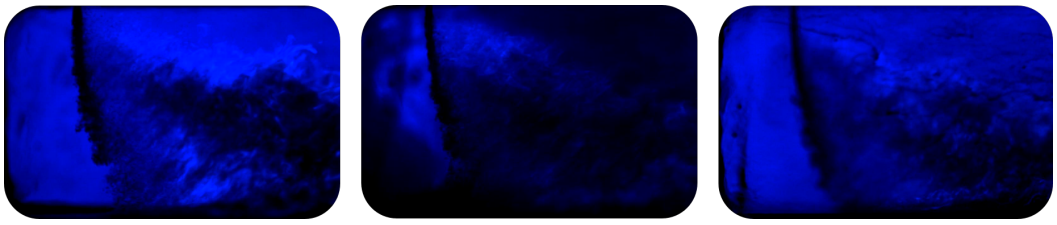

Figure 20. Flawless visualization image (**left**); image disruption by soot deposition (**middle**); and out-of-focus image (**right**).

Therefore, it was necessary to find a solution to effectively process these images so that the liquid jet trajectory could be extracted for every test case even with flaws. Figure 21 shows a conceptual diagram of imaging processing procedures for the combustion visualization images. First, the raw image obtained from the high-speed camera is converted into grayscale. Second, the intensity of the grayscale image is adjusted so that its contrast is intensified. Third, an image segmentation tool from the MATLAB® R2024a image processing toolbox is utilized using an adaptive threshold algorithm, which chooses the threshold based on the local mean intensity in the neighborhood of each pixel, to effectively distinguish the liquid column from the deposited soot and scattering droplets. Here, local graph cuts of sections are also used to generate clearer images. Lastly, the images obtained

from the recording period (1 s, approximately 4000 images) are all processed identically and then averaged over time. Lastly, the jet trajectory is extracted by manual selection and interpolation of the pixels in the liquid column. The average images and the jet trajectories for each test case are shown in Figure 22.

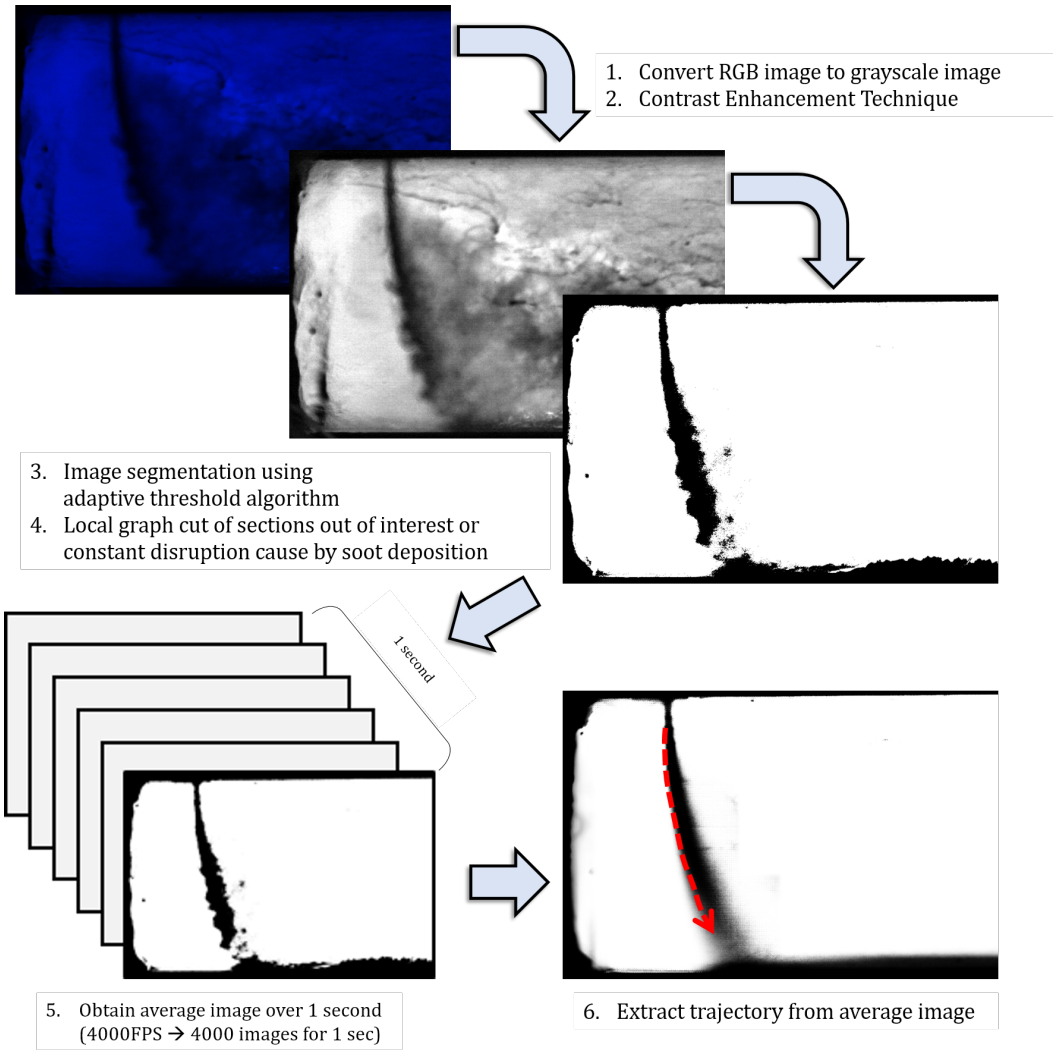

Figure 21. Conceptual diagram of imaging processing procedures for combustion visualization images.

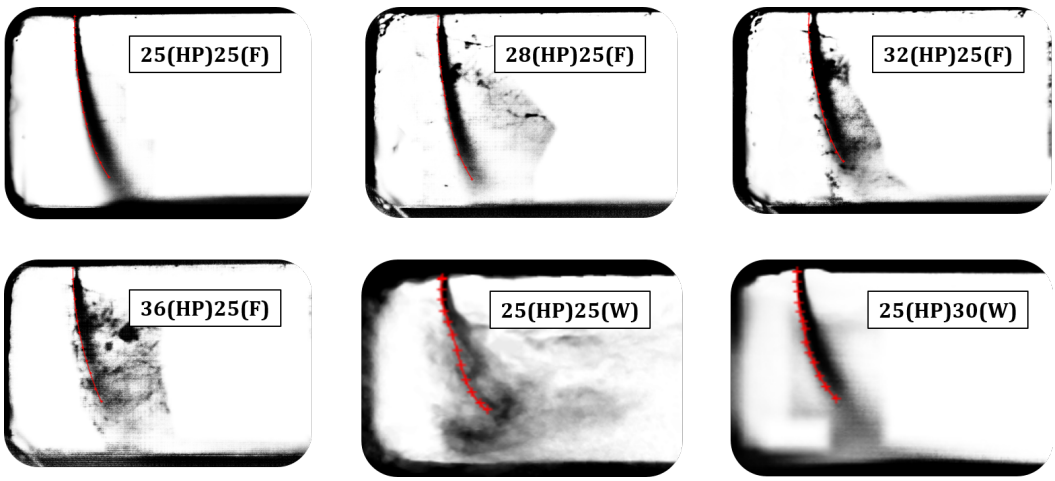

Figure 22. Average image and extracted jet trajectories in bi-mode operations.

5. Results and Discussions

The extracted trajectory data obtained from the average images shown in Figure 23 were compared with the empirical correlations suggested in past studies. Here, the errors between the actual trajectory and the predicted ones from the empirical correlations were measured using the root mean square error (RMSE). RMSE is a frequently used measure of differences between values predicted by a model or an estimator and the values observed, calculated as expressed in Equation (2).

$$\mathrm{RMSE} = \sqrt{\sum_{i=1}^{n} \frac{(z_i^R - z_i)^2}{n}} \tag{2}$$

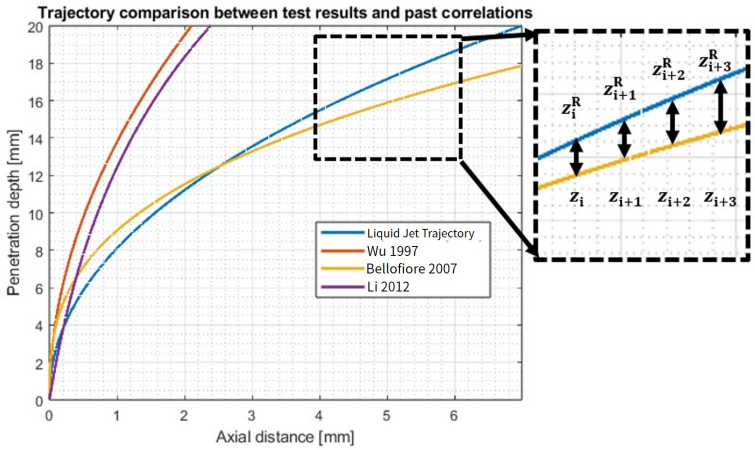

Figure 23. Trajectory comparison and RMSE calculation between observed data and past correlations [11,13,15].

5.1. Comparison with Previous Correlations

Four correlations were selected from previous studies and compared with observation data acquired from the experiments. As mentioned in Section 1, Wu's correlation [11], which is derived from the STP crossflow condition, was widely utilized in designing several H_2O_2/HC bipropellant thrusters [1,2,4]. Correlations based on high-temperature standard-pressure (HTSP, Yoon et al. [23]) and high-temperature high-pressure (HTHP, Li et al. [15] and Bellofiore et al. [13]) characteristics were also chosen for the comparison. The correlations of these references are expressed in Table 5.

Table 5. Liquid jet in crossflow trajectory correlations of previous studies.

Reference	Correlation	Range
Wu et al. [11]	$z/d_j = 1.37q^{0.5}(x/d_j)^{0.5}$	$q : 3.4 - 185$ $We_g : 57 - 1180$ $x/d_j : 0 - 12$
Yoon et al. [23]	$z/d_j = 2.241q^{0.402}(x/d_j)^{0.41}$	$q : 2 - 29.1$ $We_g : 5.3 - 47.9$ $x/d_j : 0 - 27$ $T(K) : 293, 500$
Li et al. [15]	$z/d_j = 1.44\ln(1.06(x/d_j) + 1)q^{0.4356}We_g^{0.01147}(T/T_0)^{0.295}$	$q : 16 - 76$ $We_g : 399 - 1630$ $x/d_j : 0 - 40$ $P(bar) : 5 - 20$ $T(K) : 280 - 650$
Bellofiore et al. [13]	$z/d_j = 0.909q^{0.476}(x/d_j)^{0.35}We_L^{-0.128}Re_g^{0.135}$	$q : 12.2 - 71.4$ $We_L : 10.4 - 410.5$ $x/d_j : 0 - 12$ $P(bar) : 10, 20$ $T(K) : 300, 600$

Table 6 presents the comparison results. It was found that Wu's correlation, which is most commonly employed in the design of H_2O_2/HC bipropellant thrusters, is inaccurate under combustion chamber conditions. This substantial inaccuracy is potentially due to an increase in gas viscosity resulting from high temperatures[24], as well as non-dimensional parameters extending beyond the tested range, particularly the jet-to-crossflow momentum flux ratio. It should be noted that some thruster designs in prior studies with higher thrust levels fall within the non-dimensional parameter range recommended by these correlations, potentially leading to more precise estimations. The HTSP correlation yielded more accurate estimates than STP, albeit with a significant margin of error remaining. The effect of high-temperature crossflow, including changes in viscosity, was considered, but the impact of increased pressure on aerodynamic forces and the subsequent primary breakup processes was not accounted for. In contrast to STP and HTSP condition correlations, HTHP correlations, notably those predicted by Bellofiore's correlation, were estimated with satisfactory accuracy. Both Li's and Bellofiore's correlations take into account the alterations in crossflow gas properties due to the rise in pressure and temperature. It is important to note that the discrepancy between the observed data and the predictions made using Bellofiore's correlation generally reduces with an increase in the mass flow rate of the crossflow. In simpler terms, as the jet-to-crossflow momentum flux ratio (q) diminishes, the error decreases. Bellofiore's correlation has been validated for q values ranging from 12.2 to 71.4, whereas all tested scenarios in this study exhibited q values exceeding 175. The 20(HP)25(W) test case was excluded due to an exceptionally high q of 1170.4, which falls outside the valid range. The comparison results indicate that correlations from previous research are neither accurate nor appropriate for the conditions present in the combustion chamber of the current H_2O_2/Kerosene bipropellant thruster.

Table 6. Assessment of past correlations by comparing the observed and predicted trajectories with RMSE values.

Case	Wu et al. (STP)[11]	Yoon et al. (HTSP)[23]	Li et al. (HTHP)[15]	Bellofiore et al. (HTHP)[13]
25(HP)25(F)	8.140 mm	5.569 mm	6.230 mm	0.995 mm
28(HP)25(F)	4.927 mm	3.428 mm	3.760 mm	1.228 mm
32(HP)25(F)	5.414 mm	4.045 mm	4.376 mm	0.886 mm
36(HP)24(F)	5.570 mm	4.356 mm	4.553 mm	0.888 mm
25(HP)25(W)	9.578 mm	7.539 mm	8.196 mm	3.120 mm
30(HP)25(W)	7.118 mm	5.705 mm	6.038 mm	1.774 mm

5.2. Derivation of New Correlation

A new correlation for the LIJCF suitable for use in the current design of the H_2O_2/kerosene bipropellant thruster was derived by evaluating the jet breakup positions in terms of the liquid jet (z) and gas crossflow (x) coordinates and the normalized trajectories of z/z_{jb} and x/x_{jb}. The normalized z-axis jet breakup position (z_{jb}/d_j) and the x-axis jet breakup position (x_{jb}/d_j) obtained from the combustion visualization experiments observation data were plotted as a function of a number of dimensionless parameters illustrated in Figures 24 and 25. In this study, the jet-to-crossflow momentum flux ratio $q = \rho_g u_g^2/\rho_j u_j^2$, the gas Reynolds number $Re_g = \rho_g u_g d_j/\mu_g$, and the gas Weber number $We_g = \rho_g u_g^2 d_j/\sigma$ were chosen based on previous studies [13,25]. The main difference from other LJICF studies was that we considered the effect of the radiation heat transfer from the combustion flame to the crossflow. Existing correlations failed to accurately predict both liquid jet trajectories of the fuel- and water-injected hot-fire test cases. Since the crossflow conditions were similar in terms of pressure and temperature, it seemed that the combustion process occurring downstream affects the breakdown process of the liquid jet upstream through a radiation heat transfer. Hence, to account for the effect of heat radiation from the combustion process on the jet primary breakup, a dimensionless Boltzmann number, $Bo_g = \sigma_{sb} T_{cc}^4/\rho_g C_{p,g} u_g T_g$, was implemented to the correlation. Here, σ_{sb} is the Stefan–Boltzmann constant, and T_g and T_{cc} represent the gas temperature upstream and downstream of the LJICF phenomenon, assumed to be the adiabatic decomposition temperature of the liquid hydrogen peroxide and adiabatic combustion temperature. For water injection scenarios, it was presumed that T_{cc} equaled T_g. Empirical correlations between the jet breakup positions and the dimensionless parameters were assumed to follow a general form of the power law expressed in Equation (3). Here, r_{jb} represents the jet breakup position of the coordinates, d_j is the jet orifice diameter, and the letters A to E represent the unknown parameters of the correlation that need to be fitted to the observed trajectories for each test case:

$$r_{jb}/d_j = A q^B Re_g^C We_g^D Bo_g^E \tag{3}$$

Nonlinear regression was performed to derive the empirical correlations of normalized jet breakup positions with the dimensionless parameters as expressed in Equation (4). Optimization processes were carried out using nonlinear regression using the MATLAB® Statistics toolbox to identify the five unknown parameters that best fit all datasets. The newly derived correlations indicated good agreement with experimental data with 0.965 and 0.927 as the coefficients of determination (R^2). As can be seen in Figures 24 and 25, the experimental measurements mostly sit within the 95 % confidence interval from the derived correlation.

$$\begin{aligned} z_{jb}/d_j &= 17.645 q^{0.254} Re_g^{0.241} We_g^{-0.472} Bo_g^{0.030} \\ x_{jb}/d_j &= 9.271 q^{0.230} Re_g^{0.207} We_g^{-0.614} Bo_g^{-0.053} \end{aligned} \tag{4}$$

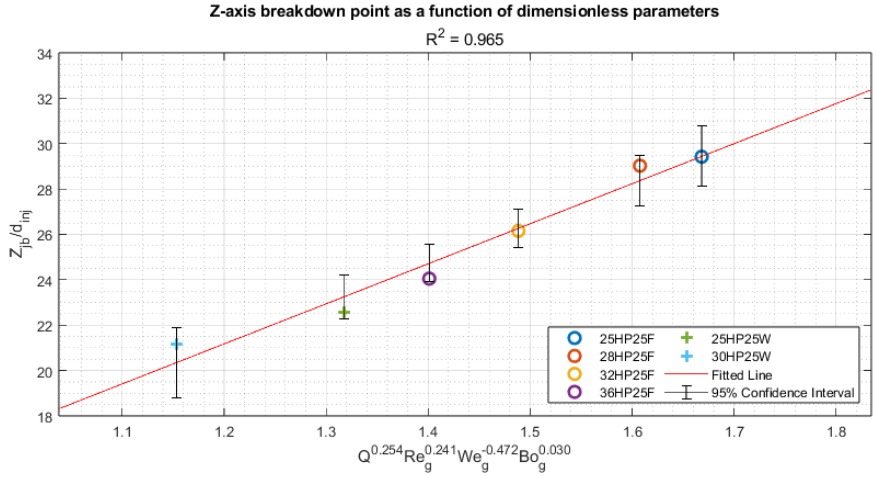

Figure 24. Z−axis breakdown position as function of dimensionless parameters.

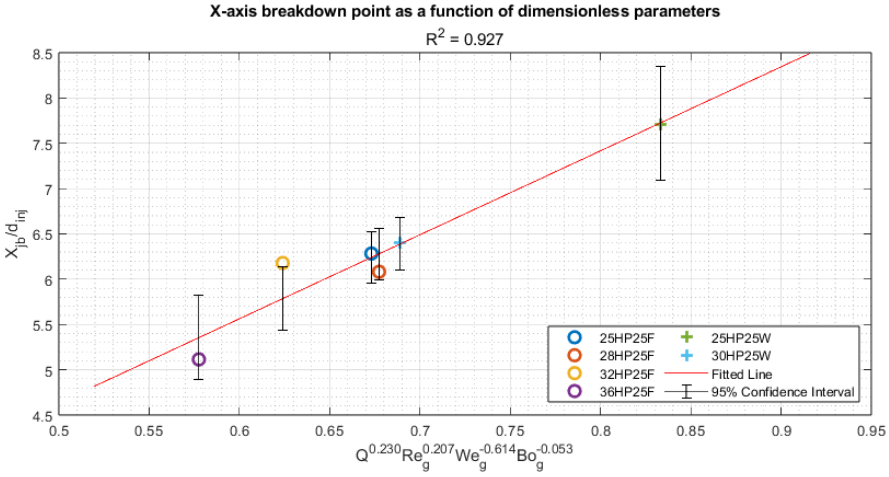

Figure 25. X−axis breakdown position as function of dimensionless parameters.

The normalized trajectories, which utilize breakup positions for each coordinate as normalizing factors, are applicable for evaluation across various operating conditions [13,25,26]. Figure 26 displays these normalized trajectories and their mean, alongside the empirical correlation formulated from the datasets. In this context, the correlation is presumed to follow a power law, which can be obtained as illustrated in Equation (5). Analogous to the earlier figures, the trajectories of the liquid jets identified in the experiments were assessed against the fitted correlation, which included a 95% confidence interval. It was found that the test cases performed during the latter stages of the test campaigns demonstrated a higher degree of error. This consistent trend is probably attributable to the challenge of precisely determining the liquid trajectories' positions due to image disturbance from soot deposition.

$$z/z_{jb} = (x/x_{jb})^{0.467} \quad (5)$$

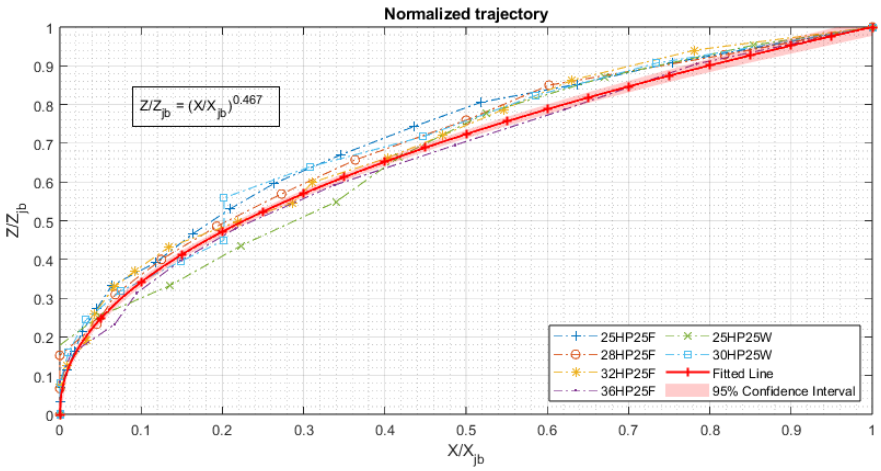

Figure 26. Normalized trajectories from the experimental data and the power law empirical correlation.

By substituting Equation (4) into Equation (5), an empirical expression can be derived for the LJIFC for H_2O_2/kerosene bipropellant thruster, as expressed in Equation (6).

$$z/d_j = 6.237 q^{0.147} Re_g^{0.144} We_g^{-0.185} Bo_g^{0.0544} (x/d_j)^{0.467}$$
$$\begin{pmatrix} q: 177.3 - 300.5, & Re_G: 102.9 - 146.0, \\ We_g: 4.339 \times 10^4 - 1.344^{\times} 10^5, & T_{cc}(K): 1053, 2526 - 2719 \\ Bo_g = 0.0138 - 0.945, & P(bar): 25 - 32 \end{pmatrix} \quad (6)$$

The RMSE for each test case and the comparison between the extracted and the predicted jet trajectories are shown in Table 7 and in Figure 27.

Table 7. Comparison between observed and predicted jet trajectory using RMSE values.

Case	Current Work	Bellofiore et al. [13]
25(HP)25(F)	0.665 mm	0.995 mm
28(HP)25(F)	0.764 mm	1.228 mm
32(HP)25(F)	0.142 mm	0.886 mm
36(HP)24(F)	0.231 mm	0.888 mm
25(HP)25(W)	0.737 mm	3.120 mm
30(HP)25(W)	0.612 mm	1.774 mm

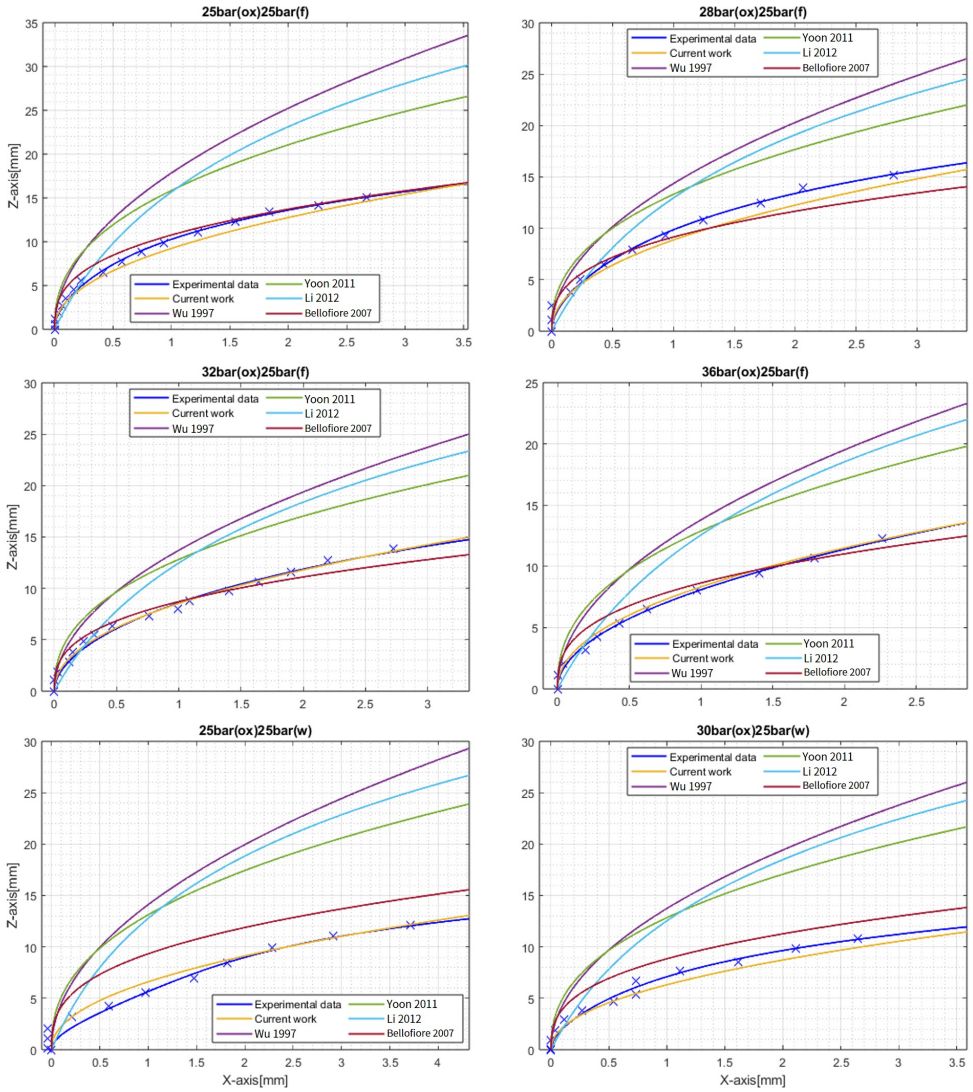

Figure 27. Comparison between predictions of previous correlations and newly derived correlation [11,13,15,23].

6. Conclusions

The LJICF phenomenon was observed through combustion visualization using the chemiluminescence-suppressed shadowgraph technique in the H_2O_2/Kerosene bipropellant thruster. A combustion chamber with an optical window and N_2 gas film cooling was designed and fabricated for the hot-fire tests. The hot-fire tests were conducted in two different test campaigns, each injecting Jet A-1 and water through the transverse fuel injector. The raw images obtained from the hot-fire tests visualization were edited with a series of image processing steps to extract the liquid jet trajectory data. A comparison between the observed and the predicted trajectories based on past studies revealed that the prior thruster designs may be based on inaccurate empirical correlations. This is likely due to a failure to consider the elevated viscosity of the high-temperature crossflow, along with the additional rise in crossflow temperature brought about by radiation heat transfer from the subsequent combustion process. It is worth noting that the thruster design of the current study accompanies a higher jet-to-crossflow momentum flux ratio than most of the past empirical correlations. Thus, past thruster designs may not have experienced such drastic differences between the intended and the actual liquid jet trajectory as suggested in this study. In any case, compensating the LJICF prediction could contribute to the optimal design and performance improvement of the propulsion system. Therefore, a new corre-

lation accounting for the HTHP crossflow and the heat transfer from the flame radiation was derived based on the observation data obtained from the hot-fire tests. Through a multi-objective optimization process using nonlinear regression, it was possible to derive an empirical correlation that achieves high accuracy for the HTHP condition of a rocket combustion chamber with or without the trailing combustion process. The novel correlation developed in this study was both derived from and validated using the H_2O_2/Kerosene propellant combination. Consequently, careful consideration is required before applying this correlation to alternative propellant combinations. Moreover, the current study involved a limited number of test cases, and future research is expected to increase the dataset to formulate more precise correlations.

Author Contributions: Conceptualization, S.M.C. and S.J.; formal analysis, S.M.C.; funding acquisition, S.M.C. and S.K.; investigation, S.M.C., V.M.P.U. and S.J.; methodology, S.M.C.; project administration, S.M.C. and S.K.; software, S.M.C.; supervision, S.K.; validation, S.M.C.; visualization, S.M.C., V.M.P.U. and S.J.; writing—original draft, S.M.C. All authors have read and agreed to the published version of the manuscript.

Funding: This work was supported under the framework of an international cooperation program managed by the National Research Foundation of Korea (NRF-2023K2A9A2A1500018011, FY2023).

Data Availability Statement: The data presented in this study are available on request from the corresponding author.

Conflicts of Interest: No conflicts of interest are associated with the work of this manuscript, and the manuscript has been approved by all authors for publication. I would like to declare on behalf of my co-authors that the work described was original research that has not been published previously, and is not under consideration for publication elsewhere, in whole or in part. All authors have read and agreed to the published version of the manuscript.

References

1. Miller, K.; Sisco, J.; Austin, B.; Martin, T.; Anderson, W. Design and Ground Testing of a Hydrogen Peroxide/Kerosene Combustor for RBCC Application. In Proceedings of the 39th AIAA/ASME/SAE/ASEE Joint Propulsion Conference and Exhibit, Huntsville, AL, USA, 20–23 July 2003. https://doi.org/10.2514/6.2003-4477.
2. Sisco, J.; Mok, J.; Austin, B.; Anderson, W. Autoignition of Kerosene by Decomposed Peroxide in a Dump Combustor Configuration. In Proceedings of the 39th AIAA/ASME/SAE/ASEE Joint Propulsion Conference and Exhibit, Huntsville, AL, USA, 20–23 July 2003; Volume 21. https://doi.org/10.2514/6.2003-4921.
3. Jo, S.; An, S.; Kim, J.; Yoon, H.; Kwon, S. Performance Characteristics of Hydrogen Peroxide/Kerosene Staged-Bipropellant Engine with Axial Fuel Injector. *J. Propuls. Power* **2011**, *27*, 684–691. https://doi.org/10.2514/1.B34083.
4. Heo, S. Design and Validation of Hydrogen Peroxide/Kerosene Bipropellant Thruster. Ph.D. Thesis, Korea Advanced Institute of Science and Technology, Daejeon, Republic of Korea, 2018.
5. Jang, D.; Kwak, Y.; Kwon, S. Design and Validation of a Liquid Film-Cooled Hydrogen Peroxide/Kerosene Bipropellant Thruster. *J. Propuls. Power* **2015**, *31*, 761–765. https://doi.org/10.2514/1.B35434.
6. Okninski, A.; Bartkowiak, B.; Sobczak, K.; Kublik, D.; Surmacz, P.; Rarata, G.; Marciniak, B.; Wolanski, P. Development of a Small Green Bipropellant Rocket Engine Using Hydrogen Peroxide as Oxidizer. In Proceedings of the 50th AIAA/ASME/SAE/ASEE Joint Propulsion Conference, Cleveland, OH, USA, 28–30 July 2014; pp. 1–10. https://doi.org/10.2514/6.2014-3592.
7. Cieśliński, D.; Okniński, A.; Ranachowski, M.; Sekrecki, M.; Bartkowiak, B.; Surmacz, P.; Kutnik, K.; Gorgeri, A.; Marciniak, B.; Borys, M. Liquid throttleable engine utilizing high-test peroxide - green storable propulsion solution for future space transportation. In Proceedings of the International Astronautical Congress, IAC, Paris, France, 18–22 September 2022; Volume 2022-Septe.
8. Surmacz, P.; Sobczak, K.; Bartkowiak, B.; Rarata, G.; Okninski, A.; Mayer, T.; Wolanski, P.; Bel, F.V. Development status of 500 N—Class HTP/TMPDA Bi-propellant rocket engine. In Proceedings of the International Astronautical Congress, IAC, Bremen, Germany, 1–5 October 2018; Volume 2018-Octob, pp. 1–5.
9. Okninski, A.; Kindracki, J.; Wolanski, P. Multidisciplinary optimisation of bipropellant rocket engines using H_2O_2 as oxidiser. *Aerosp. Sci. Technol.* **2018**, *82–83*, 284–293. https://doi.org/10.1016/j.ast.2018.08.036.

10. Santi, M.; Fagherazzi, M.; Barato., F.; Pavarin., D. Design and testing of a hydrogen peroxide bipropellant thruster. In Proceedings of the AIAA Propulsion and Energy 2020 Forum, Virtual Event, 24–28 August 2020; pp. 1–18. https://doi.org/10.2514/6.2020-3827.
11. Wu, P.K.; Kirkendall, K.A.; Fuller, R.P.; Nejad, A.S. Breakup Processes of Liquid Jets in Subsonic Crossflows. *J. Propuls. Power* **1997**, *13*, 64–73. https://doi.org/10.2514/2.5151.
12. Broumand, M.; Birouk, M. Liquid jet in a subsonic gaseous crossflow: Recent progress and remaining challenges. *Prog. Energy Combust. Sci.* **2016**, *57*, 1–29. https://doi.org/10.1016/j.pecs.2016.08.003.
13. Bellofiore, A.; Cavaliere, A.; Ragucci, R. Air density effect on the atomization of liquid jets in crossflow. *Combust. Sci. Technol.* **2007**, *179*, 319–342. https://doi.org/10.1080/00102200600809563.
14. Masuda, B.J.; McDonell, V.G. Penetration of a recessed distillate liquid jet into a crossflow at elevated pressure and temperature. In Proceedings of the 10th International Conference on Liquid Atomization and Spray Systems, ICLASS 2006, Kyoto, Japan, 27 August–1 September 2006.
15. Li, L.; Lin, Y.; Xue, X.; Gao, W.; Sung, C.J. Injection of liquid kerosene into a high-pressure subsonic air crossflow from normal temperature to elevated temperature. In Proceedings of the ASME Turbo Expo, Turbine Technical Conference and Exposition, Copenhagen, Denmark, 11–15 June 2012; American Society of Mechanical Engineers: New York, NY, USA, 2012; Volume 2, pp. 877–884. https://doi.org/10.1115/GT2012-69241.
16. Eslamian, M.; Amighi, A.; Ashgriz, N. Atomization of Liquid Jet in High-Pressure and High-Temperature Subsonic Crossflow. *AIAA J.* **2014**, *52*, 1374–1385. https://doi.org/10.2514/1.J052548.
17. Amighi, A.; Ashgriz, N. Trajectory of a Liquid Jet in a High Temperature and Pressure Gaseous Cross Flow. *J. Eng. Gas Turbines Power* **2019**, *141*, 1–11. https://doi.org/10.1115/1.4042817.
18. U.S. Department of Defense. *Propellant, Hydrogen Peroxide*; Technical Report; U.S. Department of Defense: Washington, DC, USA. 1968.
19. Gordon, S.; McBride, B.J. *Computer Program for Calculation of Complex Chemical Equilibrium Compositions and Applications*; Technical Report; NASA: Houston, TX, USA, 1994.
20. Jung, S.; Choi, S.; Kwon, S. Design Optimization of Green Monopropellant Thruster Catalyst Beds Using Catalytic Decomposition Modeling. In Proceedings of the 53rd AIAA/SAE/ASEE Joint Propulsion Conference, Atlanta, GA, USA, 10–12 July 2017; pp. 1–10. https://doi.org/10.2514/6.2017-4924.
21. Jung, S.; Kim, K.S.; Kwon, S. Combustion Performance Enhancement of a Hydrogen Peroxide Bi-propellant Thruster Using the Fluidic Oscillator Kerosene Injector. In Proceedings of the International Astronautical Congress, IAC, Paris, France, 18–22 September 2022; Volume 2022-Septe.
22. Harrje, D.T.; Reardon, F.H. *Liquid Propellant Rocket Combustion Instability. NASA SP-194*; Technical Report; Scientific and Technical Information Office, National Aeronautics and Space Administration: USA, 1972. Available online: https://ntrs.nasa.gov/citations/19720026079 (accessed on 27 December 2024). https://doi.org/10.2514/8.4111.
23. Yoon, H.J.; Hong, J.G.; Lee, C.W. Correlations for penetration height of single and double liquid jets in cross flow under high-temperature conditions. *At. Sprays* **2011**, *21*, 673–686. https://doi.org/10.1615/AtomizSpr.2012004212.
24. No, S.Y. Empirical Correlations for Penetration Height of Liquid Jet in Uniform Cross Flow—A Review. *J. ILASS-Korea* **2011**, *16*, 176–185.
25. Ragucci, R.; Bellofiore, A.; Cavaliere, A. Statistical evaluation of dynamics and coherence breakdown of kerosene and water jets in crossflow. In Proceedings of the 19th Annual Conference on Liquid Atomization and Spray Systems (ILASS-Europe'04), Nottingham, UK, 6–8 September 2004; pp. 44–49.
26. Chen, T.; Smith, C.; Schommer, D.; Nejad, A. Multi-zone behavior of transverse liquid jet in high-speed flow. In Proceedings of the 31st Aerospace Sciences Meeting, Reno, NV, USA, 11–14 January 1993. https://doi.org/10.2514/6.1993-453.